Adsorption of Cyanine Dyes on Gold Nanoparticles and Formation of J-Aggregates in the Nanoparticle Assembly

I-Im S. Lim,[†] Frank Goroleski,[‡] Derrick Mott,[†] Nancy Kariuki,[†] Wui Ip,[†] Jin Luo,[†] and Chuan-Jian Zhong*,[†]

Department of Chemistry, State University of New York at Binghamton, Binghamton, New York 13902, and Crysta-lyn Chemical Inc., Binghamton, New York 13902

Received: December 30, 2005; In Final Form: February 9, 2006

This paper describes the results of an investigation of the interparticle interactions and reactivities in the assembly of gold nanoparticles mediated by cyanine dyes. The combination of the positively charged indolenine cyanine dyes and the negatively charged gold nanoparticles is shown to form a J-aggregate bridged assembly of nanoparticles, in addition to hydrophobic interparticle and electrostatic dye−particle interactions. Such interparticle interactions and reactivities are studied by probing the absorption of J-aggregates and fluorescence from the dyes and the surface plasmon resonance absorption from the nanoparticles. The J-aggregation of the dyes adsorbed on the nanoparticles is shown to play an important role in the assembly of nanoparticles. The spectral evolution of the J-band of the dyes and the surface plasmon resonance band of the nanoparticles was found to be sensitive to the nature of the charge and the structure of the dyes. The fluorescence quenching for the dyes was shown to be quantitatively related to the surface coverage of the dyes on the nanocrystal surfaces. These findings have provided important information for assessing a two-step process involving a rapid adsorption of the dyes on the nanoparticles and a subsequent assembly of the nanoparticles involving a combination of interparticle J-aggregation and hydrophobic interactions of the adsorbed dyes. The results are discussed in terms of the structural effects of the dyes, and the interparticle molecular interactions and reactivities, which provide important physical and chemical insights into the design of dye−nanoparticle structured functional nanomaterials.

Introduction

The understanding of interparticle interactions and reactivities of metal or semiconductor nanoparticles in the presence of chemical or biological species is a challenging area in the exploitation of the optical or electrical properties for spectroscopic nanoprobes and photochemical or sensory devices. Molecularly capped nanocrystals have recently attracted increasing interest in developing such an understanding because the molecular capping or linkage can act as a protective shell to resist the propensity of aggregation, and also be tailored to define the interfacial spacing and chemistry in controllable ways. There are many examples that exploit such nanostructured interfacial properties, including place-exchange reactions of ligands,[1] layer-by-layer stepwise assembly,[2] DNA linked assembly,[3] polymer- or dendrimer-mediated molecular recognition,[4,5] hydrogen-bonding-mediated assembly,[6] and multidentate-thioether-mediated assembly.[7] Molecularly mediated assemblies of nanoparticles have also been exploited for chemical sensing,[6b,8−10] catalysis,[11,12] drug delivery, nanoelectronics,[2a,13] and medical diagnostics.[3,14] As one increasingly important class of nanostructures, the immobilization of dye molecules onto nanoparticles has captured recent interest in exploiting its optical properties for chemical and biological applications, including fluorescence quenching of small dye molecules on gold nanoparticles,[15,16] complementary oligonucleotides for single stranded DNA linked metal nanoparticles or bar-coded metal nanowires,[17−19] and fluorescent-dye-doped nanoparticles for medical diagnostics and labeling.[20] The study of dye-capped metal nanoparticles has also attracted interest in various areas of basic research,[21−24] including water-soluble monolayer-protected clusters (MPCs) functionalized with tiopronin for fluorescence quenching of fluorescein and detection of DNA binding to tiopronin/ethidium MPCs[23] and molecular interactions involving electron or energy transfer for fluorescence quenching as a result of the proximity of dye molecules to the metal nanoparticle surface.[21a]

While many promising applications of the dye−nanoparticle combination emerge, the detailed understanding of the interparticle interactions and reactivities, especially in cases involving dye-mediated assemblies, is rather limited. We report herein the results of an investigation of the assembly of gold nanoparticles and cyanine dyes as a model system for the exploration of such interactions and reactivities. The system involves a combination of electrostatic and $\pi-\pi$ interactions for cyanine dyes, especially indolenine cyanine dye (ICD), which are studied by probing the unique optical properties of J-aggregates from the dyes and the surface plasmon resonance from the nanoparticles. The measurements of the optical absorption and fluorescence properties of this combination have provided important insights into the understanding of the interparticle molecular interactions and reactivities, which will be useful for the design of the dye-structured nanoprobes for different applications, including hybridization of DNAs attached with hydrophilic fluorophore cyanines for enhancing stability, specificity, and

* To whom correspondence should be addressed. E-mail: cjzhong@binghamton.edu.
[†] State University of New York at Binghamton.
[‡] Crysta-lyn Chemical Inc..

10.1021/jp057584h CCC: $33.50
Published on Web 03/14/2006

fluorescence brightness,[25] dye−TiO_2 as photosensitizer[26] and optical data storage, and fluorescence labeling as fluorescent probes (e.g., CyDyes). Such probes have a narrow bandwidth, large extinction coefficient, reasonable fluorescent quantum yield, and easy construction of bioassay format based on fluor (donor)−quencher (acceptor) by engineering the extent of the conjugation of the dyes and the donor−acceptor distance.[27]

Molecularly organized aggregates such as J- and H-aggregates are interesting because of their unique electronic and spectroscopic properties.[28] In J-aggregates, the one-dimensional arrangement is such that the transition moments of monomers are aligned parallel to the line joining their centers in an end-to-end fashion, which is different from H-aggregates where the one-dimensional arrangement is such that the transition moments of monomers are aligned parallel to each other but perpendicular to the line joining their centers in a face-to-face fashion. The most characteristic feature of J-aggregates is the red-shifted narrow absorption band (J-band) with respect to the monomer absorption, in contrast to the blue-shifted absorption band for H-aggregates. While the formation of J-aggregates is well-known for cyanine dyes[28] and a number of other dyes, the understanding of how such interactions are operative in the adsorption and assembly of nanoparticles is still limited. In recent studies,[29] nanoparticles of synthetic clay or silica coated with cyanine dyes or polymers have been shown to form J-aggregated assemblies in water, exhibiting absorption characteristics corresponding to small J-aggregate domains and fluorescence superquenching characteristics. The aggregation effect for the association of electroactive dyes onto metal nanoparticles,[21b,d] forming H-aggregates of rhodamine 6G on gold nanoparticles as a result of intermolecular interactions, has been reported by Kamat and co-workers. For silver nanoparticles capped with rhodamine 6G, H-aggregates were evidenced by the blue shifts of both the surface plasmon resonance band of the particles and the visible absorption band of the dyes.[30] Recently, photoexcitation of the surface plasmon in Ag nanoparticles coated with J-aggregates of a cyanine derivative was shown to lead to exciton dynamics different from J-aggregate monolayers on bulk metal surfaces due to a coherent coupling between the exciton of a J-aggregate and the electronic polarization of metal nanoparticles. The coherent coupling to the conduction band electrons leads to constructive interference and a long-lived exciton for Ag nanoparticles, whereas it interferes destructively with bound electron transition dipoles for Au nanoparticles.[31,32] The study of the absorption and emission spectral characteristics of eosin (a fluorescent dye) on gold nanoparticles revealed that smaller particles stimulate J-aggregation of eosin on the surface of metal particles, whereas larger particles cannot induce any kind of aggregation.[33] The study of gold nanoparticles capped with fluorescein isothiocyanate[34,35] however showed that the chemisorbed dyes do not induce any aggregation. There is a clear need to understand the interparticle interactions and reactivities by probing the changes in optical properties involving both dyes and nanoparticles. The interparticle aggregation of charged colloids in aqueous solutions is well described by two types of simple interactions: the electrostatic effect due to adsorption of cations on the negatively charged particles to reduce the formerly repulsive charges and hydrophobic interaction when amphiphilic surfactants are adsorbed on the surface of the particles. Such electrostatic interactions are well described by the Derjaguin−Landau−Vervey−Overbeek (DLVO) theory[36] based on the assumption that the sole attraction force operating between two particles is the van der Waals' attraction and the repulsion is due solely to the Coulombic interaction. The electrostatic double layer repulsion competes with van der Waals attraction. The notion that any reduction in the charge on the particles will reduce the repulsion is however oversimplistic even for nonspecific adsorbing electrolytes because adsorption and bridging may be more important, as shown in many recent examples for nanoparticle assemblies. The bridging of colloid particles by the multifunctional molecules or polymer chains via binding simultaneously to two or more colloid particles that are sufficiently separated to allow interaction to occur at particle−particle distance so that the overlap of the diffuse double layers of the particles is not significant. Understanding the various intermolecular interactions such as $\pi-\pi$ interaction in J-aggregates, in addition to the electrostatic and hydrophobic interactions, will be important for controlling different functional nanostructures, which also constitutes part of the motivation of the present work.

SCHEME 1: Structures for the Four Different Cyanine Dyes (1 (i.e., ICD), 2, 3, and 4) Studied in This Work

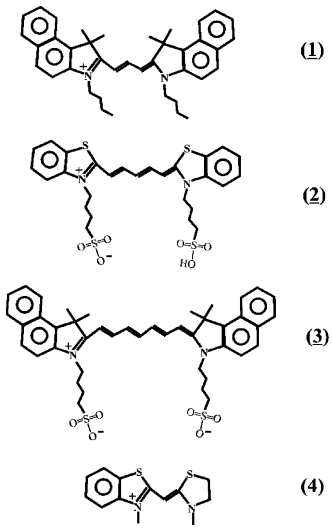

Experimental Section

Chemicals. The chemicals included hydrogen tetracholoroaurate ($HAuCl_4$, 99%), sodium citrate (Cit, 99%), and ethanol (EtOH, 99.9%). All chemicals were purchased from Aldrich and used as received. Water was purified with a Millipore Milli-Q water system.

The structures of four cyanine dyes (**1**, **2**, **3**, and **4**) are illustrated in Scheme 1, and these dyes were obtained from Crysta-lyn Chemical Inc. Details for the synthesis of the dyes have been reported.[37] We carefully characterized our ICD (**1**) using FTIR and NMR to ensure its structure and purity (see the Supporting Information).

The synthesis of citrate-capped gold nanoparticles (Au_{nm}) followed the reported procedure.[38] Briefly, aqueous $AuCl_4^-$ (1 mM) was heated to boiling under vigorous stirring in a cleaned glass flask. At reflux, an excess ($\times 3.8$) of sodium citrate (from a 38.8 mM stock solution) was quickly added to the solution. Citrate acts as both a reducing and capping agent. The color of the solution turned from pale yellow to clear and to light red. This solution was allowed to react while stirring under reflux for 30 min, after which the heating mantle was removed and the solution was stirred under room temperature for another 3 h. The particle size was determined using transmission electron microscopy.

Three synthetic conditions were used, which involved varying concentrations of $AuCl_4^-$ and citrate precursors. While the

concentration ratio between Au and citrate is kept constant (3.8× excess of citrate) for the synthesis, the amount of $AuCl_4^-$ and citrate used in the synthesis varied. Each condition produces Au_{nm} with slightly different average core sizes. Gold nanoparticles (4−20 nM) with average particle sizes of 10.6 ± 0.7, 11.5 ± 0.6, and 12.1 ± 0.5 nm were synthesized by varying the concentration of $AuCl_4^-$ between 0.25 and 1.0 mM and the concentration of citrate between 0.95 and 3.8 mM. Most of the data reported in this work are for the 11.5-nm-sized Au_{nm} unless otherwise stated.

Measurements and Instrumentation. The adsorption and assembly of Au_{nm} in the presence of various dyes were carried out under ambient conditions. Briefly, upon adding a desired amount of dye solution (in ethanol) into an aqueous solution of nanoparticles or vice versa, the solution was quickly mixed by purging for ~2 s before the measurement of UV−visible (UV−vis) spectra. Due to the solubility issue of ICD, a certain percentage of ethanol is added into the stock solution of ICD. The final concentration of ethanol in the solution ranged from 0.1 to 3%. The spectra were collected over the range 200−1100 nm with a HP 8453 spectrophotometer. A quartz cuvette with a path length of 1.0 cm was utilized. The stock concentration of gold nanoparticles was determined according to the absorbance data and the average size of the particles. As previously reported,[39] the molar absorptivity (ϵ_{Au}) for 13-nm-sized Au_{nm} particles determined in aqueous solution at the surface plasmon resonance band maximum (λ = 520 nm) was 2.01×10^8 M^{-1} cm^{-1}. For ICD, the value of $\epsilon_{dye(ICD)}$ determined at λ = 550 nm in aqueous solution was 1.15×10^5 M^{-1} cm^{-1}.

Transmission electron microscopy (TEM) was performed on a Hitachi H-7000 electron microscope (100 kV).

Fluorescence spectra were acquired with an SLM 48000s fluorometer with an MC320 monochromator. A fluorescence cuvette with a 1.0 cm path length was utilized. The spectra were collected over a range of 550−700 nm (excitation, 550 nm; emission, 608 nm). The instrument was tuned by a combination of "HV" (high voltage) and "DC" gain (direct current) settings (typically HV 750−900 and DC gain 10−100) to obtain the optimal performance in our measurements. Because the intensity is dependent on the power setting, our comparisons were for data within the same set of spectra. A direct comparison between spectra from measurements with different settings was not attempted.

FTIR spectra were acquired with a Nicolet Magna-IR 760 spectrometer with a liquid nitrogen cooled HgCdTe detector. The spectra were collected over the range of 400−4000 wavenumbers.

^{1}H NMR spectra were collected at 360 MHz on a Bruker (AC) spectrometer. Deuterated chloroform was used as the solvent.

Results and Discussion

1. Optical Absorption Properties. The reactivities of the citrate-capped gold nanoparticles with four different structures of cyanine dyes were examined. As shown in Scheme 1, the structures for the four dye molecules (**1** (i.e., ICD), **2**, **3**, and **4**) examined differ in terms of the nature of the charge and the size of the conjugated moiety. These differences are shown to exhibit profound differences in terms of the optical absorption data which characterize the reactivities of the dyes with the nanoparticles.

As shown in Figure 1A for a typical set of UV−vis spectra, the spectrum of ICD (**1**) exhibits two absorption bands at λ = 545 and 582 nm due to $\pi-\pi^*$ transitions. A weak shoulder band can also be identified at λ = ~630 nm. Upon addition of Au_{nm} into the ICD solution, the spectra reveal a dramatic spectral evolution depending on the concentration of the dye. At a high concentration of ICD (e.g., 9.8 μM), a red-shifted band is evident at 635 nm. The absorbance of this band increases in the first 30 s to a maximum and is followed by a subsequent decrease. The absorbance decrease of this band is accompanied by spectral changes in two regions. There is a gradual increase of absorbance or broadening of the band in the longer wavelength region (640−800 nm). This evolution is clearly at the expense of the absorbance decrease in the 500−600 nm region. To assess whether there is a contribution of the surface plasmon (SP) resonance band of Au_{nm} to the observed spectral evolution in the long wavelength region, the spectra for a solution of Au_{nm} with an identical concentration (0.42 nM) upon the addition of a lower concentration of ICD (0.64 μM) were compared with the spectral evolution. As shown by the dashed curves in Figure 1A, much smaller absorbance values were obtained, indicating that the above spectral evolution is basically a result of the optical absorption of the dyes due to interaction with the

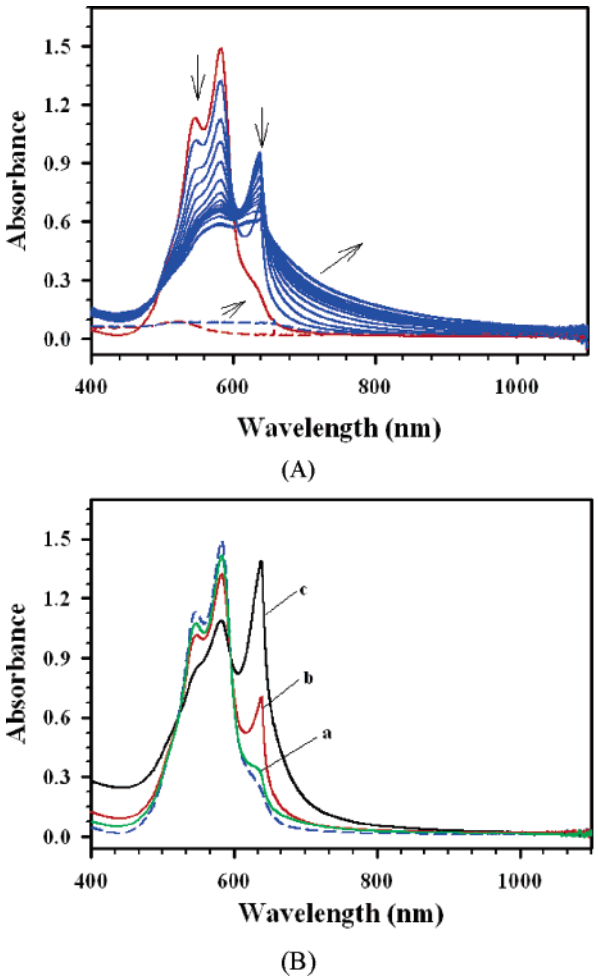

Figure 1. UV−vis spectra monitoring the ICD-mediated assembly of Au_{nm} in solutions. (A) Solid curves: spectral evolution of the $\pi-\pi^*$ bands and J-band of the dyes upon the addition of Au_{nm} into the solution of ICD ($[Au_{nm}]$ = 0.42 nM and [ICD] = 9.8 μM). Dashed curves: the change of the SP band of Au nanoparticles upon the addition of ICD into the solution of Au_{nm} ($[Au_{nm}]$ = 0.42 nM and [ICD] = 0.64 μM) (only the first and last spectra are shown). The arrow indicates the direction of the spectral evolution within the time frame of 20 min. (B) The comparison of the $\pi-\pi^*$ bands and J-band of the dyes in solutions upon adding different concentrations of Au nanoparticles, $[Au_{nm}]$ = 0 (dashed line), 0.17 (a), 0.42 (b), and 1.5 nM (c). ([ICD] = 9.6 μM). The spectra were recorded within 10 s.

SCHEME 2: Schematic Illustration of the Electrostatic and $\pi-\pi$ Interactions for the Adsorbed ICDs on Gold Nanoparticles Capped with Negatively Charged Groups (Not to Scale)

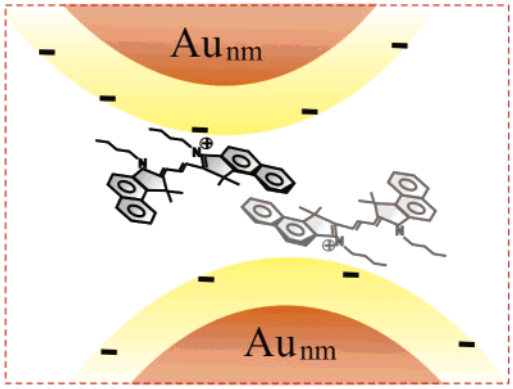

nanoparticles, ruling out the contribution of the surface plasmon resonance band of the nanoparticles. It is also found that the intensity of the band at ~630 nm is highly dependent on the concentration of Au_{nm} added to the solution. As shown in Figure 1B, the absorbance for the band at ~630 nm recorded within the first 10 s increases with the concentration of Au_{nm}. On the basis of the above observations and the red-shift characteristic, the band at ~630 nm is clearly associated with the formation of J-aggregates from the adsorbed dyes.[28a] The observation of the J-band thus demonstrates the formation of J-aggregates of the dyes as a result of the reactivities of dyes with nanoparticles (Scheme 2).

It is important to note that the observation of the peak-shaped J-aggregate band is in fact consistent with the previous experimental observation for silver nanoparticles with other cyanine dyes and the theoretical modeling of the coupling between the surface plasmon of the metal core and the molecular exciton of the dye.[31,32] A peak-shaped J-band develops when the J-band exciton absorption is located at a slightly longer wavelength than the surface plasmon resonance absorption, which is indeed the case for our dye−nanoparticle system. We also note that the red-shifted J-band for our dye−nanoparticle system, as shown in Figure 1, is initially very sharp, in agreement with the fact that the red-shifted J-band appears as an intense narrow absorption band due to the motional narrowing.[40] However, the fact that this band became relatively broad and weak in the prolonged assembly process suggests that the dye molecules could be oriented in a less optimal way of J-aggregation. Lattice disorder is often considered as one of the possible reasons for this type of reorganization.[41] Similar spectral characteristics were reported for J-aggregates of nanoparticles derived from 1-cyano-*trans*-1,2-bis-(4-methylbiphenyl)-ethylene.[40] Therefore, the initially sharp band is in agreement with the motional narrowing, whereas the subsequent broadening is due to lattice disorder as a result of the surface reorganization of the adsorbed dyes. While it is possible that there are contributions to the J-band from intermolecular (dyes on the same particle) and intramolecular (dyes between two particles) J-aggregations, which is part of our ongoing in-depth study, the observed strong dependence of the J-band intensity on the concentration of nanoparticles substantiates the formation of interparticle J-aggregations.

It is important to emphasize that, for the two dye concentrations in the above data, that is, high (e.g., 9.8 μM) and low (e.g., 0.64 μM) concentrations, the high-concentration case shows two bands from the dye molecules, whereas the low-concentration case shows one band from the Au nanoparticles. The bands from the dye are too weak to be seen in the latter case. Gold nanoparticles exhibit a strong surface plasmon resonance band at ~520 nm, the wavelength and absorbance of which strongly depend on the size, shape, interparticle distance, and surrounding dielectric medium constant.[7,42] Figure 2 shows a representative set of spectral evolution for ICD-mediated assembly of Au_{nm} in solutions of different concentrations of ICDs and Au_{nm}. It is important to point out that while the spectral evolution for both the J-band of the dyes and the SP band of the nanoparticles appears at the higher-wavelength region, they are distinctively different in band shape and intensity. There are three general characteristics for the SP band evolution. First, upon addition of ICDs to the solution, new bands emerge at wavelengths longer than the SP band of Au_{nm}. A band emerges at 680 nm accompanying the decrease of the 520 nm band. Both the band at 520 nm and the band at ~630 nm are from the SP band of Au nanoparticles, not from the dye molecules. A clear isosbestic point is observed at 660 nm, indicating the reactivity involving two species (reactant and product). Second, the wavelength for the new bands is strongly dependent on the concentration of dye. The higher the dye concentration, the longer the wavelength of the new bands. Third, at a relatively higher concentration of dye, the increase and broadening of the new bands are accompanied by a decrease of the SP band of Au_{nm}. The dependence of the spectral properties on the concentration of Au_{nm} was also examined (Figure 2C and D). The general characteristic of the spectral evolution showed some similarities, including an increase in absorbance for the new band at ~620 nm, which is accompanied by a distinct color change from red to purple. A close examination reveals however subtle differences. For example, the absorbance for the SP band of Au_{nm} at 520 nm remained largely unchanged. The spectral evolution is indicative of the formation of larger-sized assemblies of nanoparticles. The solution changed from red to purple at lower concentration, which remained soluble after 5 h, and from red to blue at higher concentration, which precipitated within 30 min.

The comparison of the spectral evolution data for several different dyes (see the Supporting Information) provided important insights for assessing the structural effects. First, the use of a cyanine dye with a similar structure but different charges, for example, neutral (i.e., **2**) and negatively charged (i.e., **3**) dyes, did not lead to any observable reactivity. The absence of any spectral evolution is due to the lack of electrostatic interaction between the dye molecule and the nanoparticles, demonstrating the important role played by the electrostatic interaction in the reactivity. The addition of NaCl (10 mM) to the solution of Au_{nm} and dye (**3**) also failed to cause any observable aggregation of the nanoparticles. Second, the use of a cyanine dye with a similar structure but smaller π-systems on both ends of the molecule (e.g., **4**) did not show observable spectral evolution under the same experimental conditions as in the case of the measurement for dye **1**. It showed observable spectral evolution only when a much higher concentration of the dye (>3×) was used. This finding suggests that, in addition to electrostatic interaction, other molecular interactions (e.g., $\pi-\pi$ interaction) involving the dye molecules have also played an important role in the spectral evolution.

To further demonstrate that the electrostatic interaction is not the only factor contributing to the spectral evolution and the driving force for the assembly process, experiments using other different positively charged molecules were performed. Examples of such molecules included tetramethylammonium

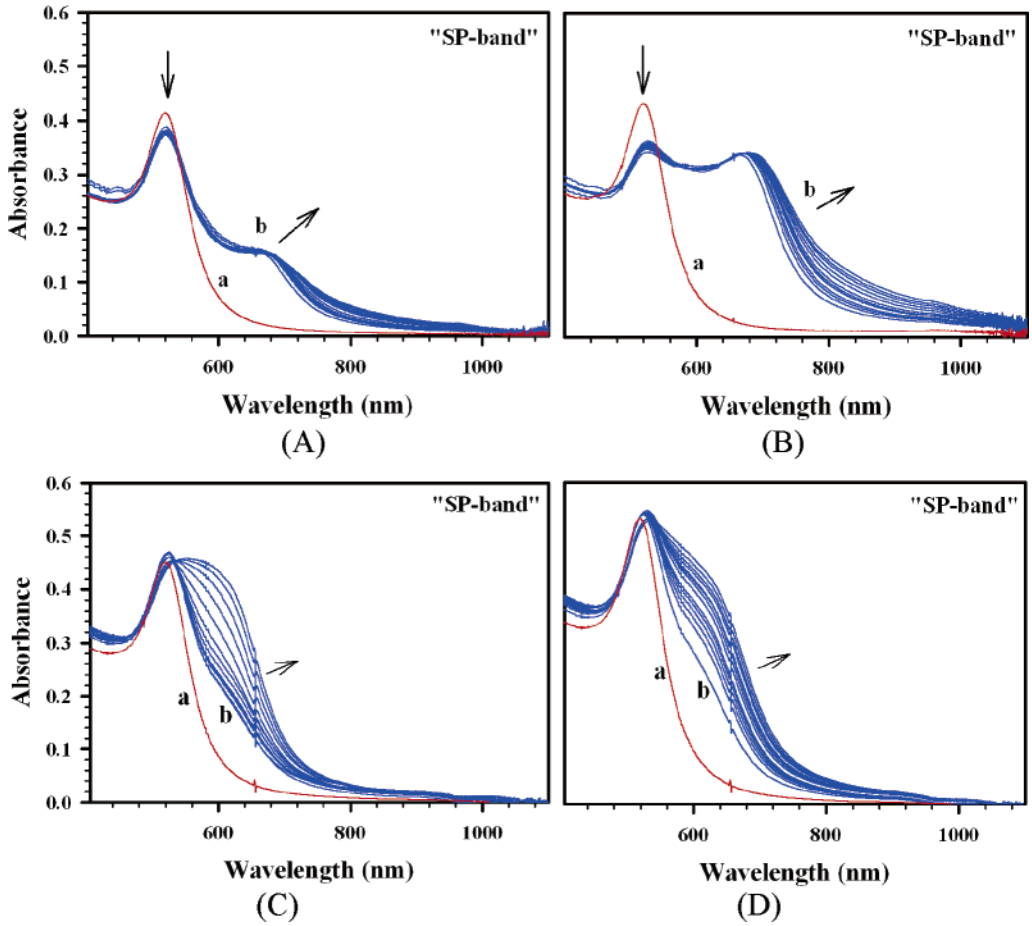

Figure 2. UV−vis spectra monitoring the SP band of the ICD-mediated assembly of Au_{nm} in solutions. (A and B) [Au_{nm}] = 2.0 nM with different concentrations of dye, [ICD] = 0.16 (A) and 0.33 μM (B) (with 0.2% ethanol); (C and D) [ICD] = 0.17 μM (with 3% ethanol) with different concentrations of Au_{nm}, [Au_{nm}] = 4.0 (C, 10.6 nm Au_{nm}) and 2.7 nM (D, 12.1 nm Au_{nm}). The curves labeled by "a" are for Au_{nm} before the addition of ICD, and the curves labeled by "b" are for Au_{nm} upon the addition of ICD (the arrow indicates the direction of the spectral evolution within the time frame of 45 min).

bromide and tetrabutylammonium tetrafluoroborate, both of which have a strong ion-pairing effect with negatively charged groups and also are relatively hydrophobic. The results of these experiments did not show any spectral evolution, even at much higher concentrations (see the Supporting Information), demonstrating that the spectral evolution for the ICD−Au_{nm} assembly is not simply due to the surface neutralization effect. Since the presence of electrolytes often exerts a specific intermediate bridging role in addition to any nonspecific double compression, this issue is further assessed by studying the spectral evolution as a function of salt concentration (e.g., 0.001−0.01 M NaCl; see the Supporting Information). No spectral evolution was detected in this concentration range in the absence of ICD dyes. Note that this salt concentration range is much higher than the dye concentration (<1 μM). The ratio of [ICD] to [Au_{nm}] used in the experiment was ~83, which translates to ~0.1 positively charged nitrogen anchored on ICD per citrate group capped on Au_{nm} (ICD has 1 positive charge, while the ~11.5 nm Au_{nm} can theoretically accommodate 1250 citrate molecules), suggesting that the amount of positive charges is 1 order of magnitude lower than the negative charges on the nanocrystal surfaces. The experimental data (in the Supporting Information) showed that, as the salt concentration increased, the spectral evolution displayed a trend of a subtle shift of the ~700 nm band toward longer wavelength, indicating the formation of increased assembly. It is well-known that the effective diffuse double layer thickness is inversely proportional to the square root of the electrolyte concentration. A higher salt concentration compresses the Debye radius (screening distance) and reduces the interparticle separation distance. At a low salt concentration, the double layer is less compact; at a high salt concentration, the double layer is more compact. The fact that the dye molecules can disrupt the compact diffuse double layer of ions and solvating molecules and lead to more extensive assembly demonstrates that the electrostatic interaction between the positively charged dyes and the negatively charged nanoparticles is indeed facilitated by the presence of salt, leading to the subsequent interparticle interactions via a combination of the $\pi-\pi$ interaction and the hydrophobic interaction of the dyes on the nanocrystal surfaces.

On the basis of the optical absorption data, a sequential two-step assembly process is believed to be responsible for the overall spectral evolution: (1) adsorption of ICD on gold nanoparticles largely driven by electrostatic interaction and (2) interparticle linkage of the ICD-capped nanoparticles largely driven by a combination of J-aggregation and hydrophobic interactions. The latter step must be a slow process, as evidenced by the gradual spectral evolution and its concentration dependence. The reason for the slow assembly is associated with the formation of J-aggregates of the adsorbed ICDs via $\pi-\pi$ interactions[28a] and was confirmed by the J-band, as shown in Figure 1. For the first step, it is a direct adsorption of the positively charged ICD on the negatively charged Au_{nm}, which does not involve the exchange of ligands with the capping molecules. Details of the reactivity will be discussed in a later section based on the measurement of the fluorescence properties of the dyes.

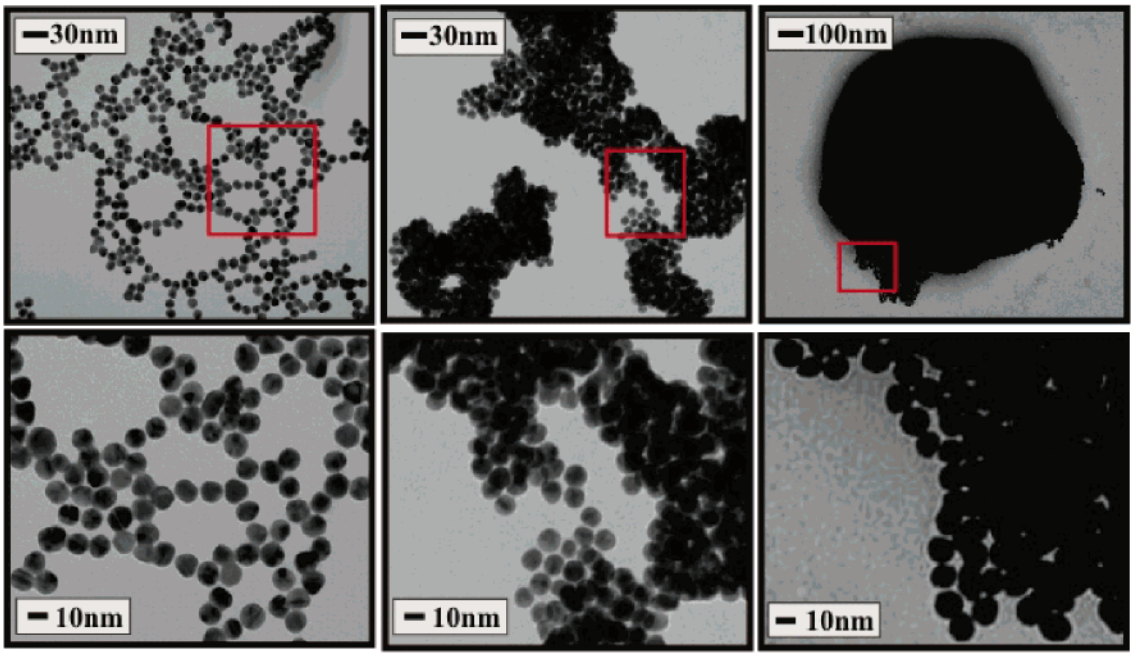

Figure 3. TEM images for samples of the ICD-mediated assembly of Au_{nm} in solutions with different concentrations of dye: [ICD] = 0 (A), 0.16 (B), and 0.31 μM (C). [Au_{nm}] = 3.1 nM.

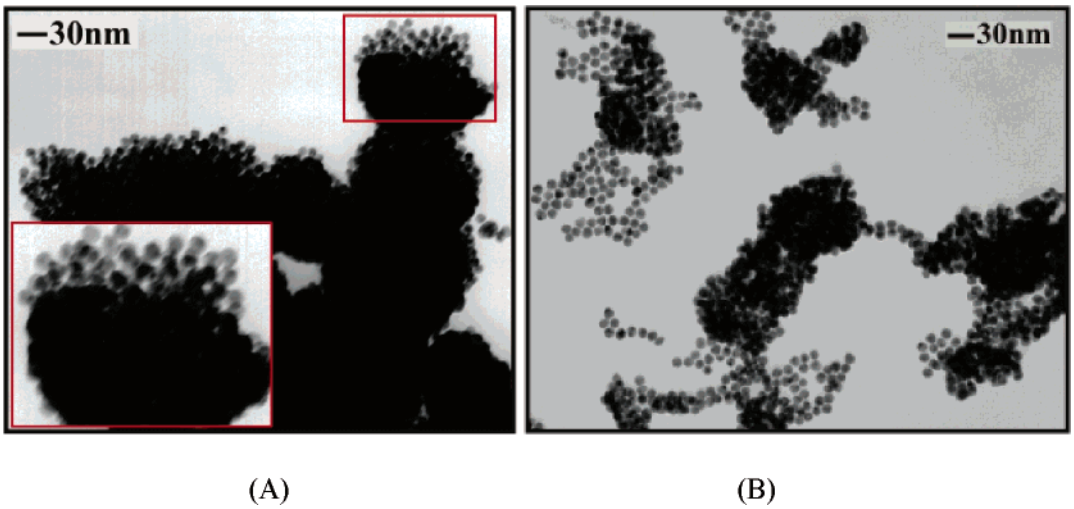

Figure 4. TEM images of ICD-mediated assembly: (A) with [Au_{nm}] = 7.9 nM and [ICD] = 0.31 μM ($r \sim 39$) (the inset shows a magnified view); (B) with [Au_{nm}] = 4.0 nM and [ICD] = 0.17 μM.

2. Morphological and Structural Properties. Upon completion of the ICD−nanoparticle assembly reaction as reflected by the leveling off of the spectral evolution, the solution was briefly sonicated and samples were taken from the solution and examined using TEM. Figure 3B and C shows a representative set of TEM images for ICD-mediated assembly of Au_{nm} derived from different concentrations of ICDs. The TEM image for Au_{nm} in the absence of ICD (Figure 3A) is included for comparison. In contrast to the fractal or chainlike features for Au_{nm} solution in the absence of ICD (Figure 3A), the samples taken from the solutions after adding ICD reveal features of highly clustered nanoparticles (Figure 3B and C). Domains of the clusters with ~50 (Figure 3B) and ~800 nm (Figure 3C) have been observed by varying the ICD concentration, 0.16 (Figure 3B) and 0.31 μM (Figure 3C), respectively. The presence of individual nanoparticles along the edges of the larger clusters and the absence of free nanoparticles are indicative of the formation of assemblies of nanoparticles with an effective interparticle linkage. The size of the cluster and the 3D packing of particles in the cluster showed an apparent increase with an increase of the ICD concentration.

The clustering morphological features are further evidenced by a sample taken from the solution of ICD-mediated assembly of Au_{nm} with a higher concentration (with a slightly different core size (~10.6 nm core size)) (Figure 4A). In this case, the dye-mediated assembly exhibits spherically shaped clusters of nanoparticles. A close examination of the clustered nanoparticles reveals the presence of certain interparticle ordering, as evidenced by the features along the edge of the clusters. Additional fine morphological features have also been observed by varying the concentration of nanoparticles. Figure 4B shows another representative set of TEM images for ICD-mediated assembly of Au_{nm} under the conditions corresponding to the spectral evolution shown in Figure 2C. Because of the relatively low

concentration of ICD, the assemblies were soluble for weeks before precipitation occurred. From the ordered domains of nanoparticles around the large clusters or in the smaller clusters, the interparticle edge-to-edge distance was found to display an average value of 1.8 ± 0.5 nm, which is larger than that found for citrate-capped Au_{nm} particles (~1.3 nm). The increased interparticle distance reflects the presence of ICD molecules between the nanoparticles. Structurally, the long dimension of the ICD molecule is ~2.5 nm, whereas the width and thickness dimensions are ~1.5 and ~0.5 nm. The usual distance for $\pi-\pi$ interactions is ~0.4 nm. By comparing these values with the interparticle distance measured (1.8 nm), two conclusions can be found. First, the nanoparticles in the assembly are individually isolated, which is consistent with the picture of molecular bridging between the nanoparticles as revealed by the adsorption data, and in contrast to those known for simple salt-induced aggregation of nanoparticles in which the nanoparticles are usually fused together because of the collapse of electrical double layers. Second, the dye molecules are likely oriented so that $\pi-\pi$ interaction along the thickness dimension of the dye is responsible for bridging the neighboring nanoparticles.

We also performed FTIR characterization of the nanoparticle assemblies to assess the interparticle structural properties. The results (see the Supporting Information) for ICD-mediated assembly of Au_{nm} revealed some similarities and differences in comparison with the spectral features for ICD and Au_{nm}. For example, the band detected for the asymmetric stretching mode of carboxylate seemed to be strong and clearly shifted to 1633 cm^{-1}. One possible explanation is the strong interaction between the carboxylate and the positively charged ammonium moiety of ICD, in contrast to the weak interaction with its counterion (Na^+). The band observed at 1460 cm^{-1} could be due to the symmetric stretching mode of carboxylate, mixed with some CH bending component from methylene groups. The band observed around 1378 cm^{-1} could be assigned to part of the CH bending modes on the aromatic ring. Overall, features corresponding to the citrate molecules are predominant, whereas features from the dye molecules do not appear to be significant in terms of absorbance. Two possible scenarios include (1) the presence of a relatively small fraction of dye in the assembly in comparison with the capping citrate molecules and (2) the strong $\pi-\pi$ interaction of the aromatic rings influencing some of the vibrational properties. While an in-depth understanding of these two scenarios (e.g., using Raman spectroscopy) is part of our ongoing work, the fluorescence quenching data as presented in the next section provided important information for assessing the adsorption of dye molecules on the nanoparticles.

3. Fluorescence Quenching Properties. While ICD is highly fluorescent, the ICD−Au_{nm} assembly was found to display fluorescence quenching properties, which provided an important means for assessing the mechanistic details of the interparticle interactions for the nanoparticle assembly. Figure 5 shows a representative set of fluorescence spectral changes for a solution of ICD upon the addition of Au_{nm}. An important finding in this experiment is that the fluorescence quenching of ICD occurs almost immediately (<1 min), which is in contrast to the gradual UV−vis spectral evolution for the dye-mediated assembly of nanoparticles. The rapid quenching is suggestive of a rapid adsorption of ICDs on Au_{nm}, whereas the slow colorimetric change reflects the slower interparticle ligand interaction following the ligand adsorption. The quenching is due to energy transfer as a result of the adsorption of ICD on Au_{nm}. Previous studies have shown that the fluorescence quenching is dependent

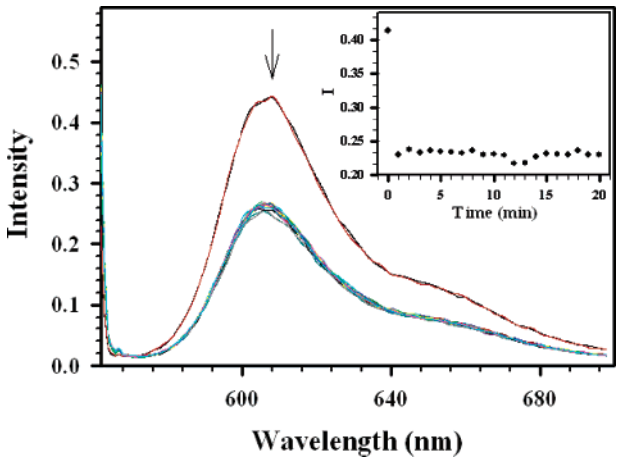

Figure 5. Florescence spectra of ICD upon the addition of Au_{nm}. [Au_{nm}] = 0.32 nM, and [ICD] = 1.0 μM. Each spectrum was taken with an increment of 1 min over a time length of 20 min. Inset: plot of intensity (I) at 608 nm vs time. The arrow indicates the direction of the spectral evolution.

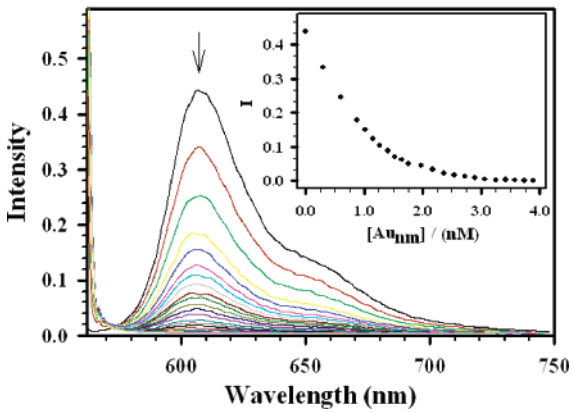

Figure 6. Fluorescence spectra of ICD (initial concentration 1 μM) upon the addition of Au_{nm} (12.6 nM) with an increment of either 25 or 50 μL. Each spectrum was recorded 5 min after the addition of Au_{nm}. Inset: plot of the intensity (I) at 606 nm vs the concentration of Au_{nm}. The arrow indicates the direction of the spectral evolution.

on the distance between the dye and the metal particle surface. Quenching usually occurs at a distance of a few nanometers (< ~5 nm) by Foster energy transfer from the fluorophore to the surface plasmon resonance absorption of the metal particles.[24] In our case, the distance between Au_{nm} and ICD is defined by a combination of the electrostatic and $\pi-\pi$ interactions between the negative citrate and the positive cyanine groups, which is approximately 1.8 nm and falls in the range known for fluorescence quenching.

The fluorescence quenching is found to be quantitatively related to the adsorption of dye on Au_{nm}. Figure 6 shows a representative set of fluorescence data obtained by incrementally adding Au_{nm} solution to the ICD solution. In this experiment, the total amount of moles of ICD (2×10^{-9} mol) was kept constant while its concentration was diluted (1.45×) by the added volumes of Au_{nm}. The dependence of fluorescence quenching on the quantity of Au_{nm} is clearly evidenced by the decrease of the fluorescence intensity as a function of the amount of Au_{nm}. This type of dependence is also reminiscent of quantitative titration of dye molecules by Au_{nm}. Assuming that the quenching only occurs for those ICDs that have direct interaction with the Au_{nm} surface, the maximum of the quenched ICDs is then restricted to a full monolayer coverage of ICD on the nanoparticle surface, which depends on the orientation of

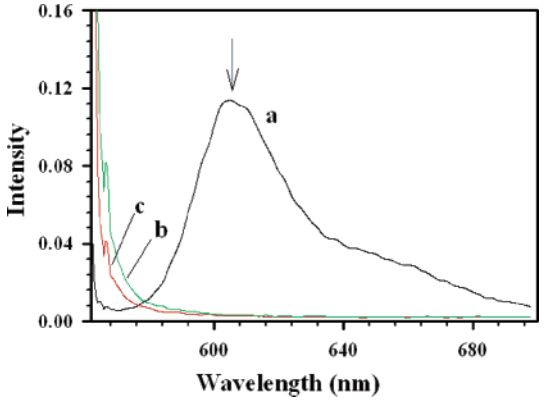

Figure 7. Fluorescence spectra showing quenching efficiency using Au_{nm} of different concentrations ([Au_{nm}] = 0 (a), 3.9 (b), and 7.8 nM (c)), [ICD] = 0.67 μM. The arrow indicates the direction of the spectral evolution.

the adsorbed ICD. A lower limit coverage would be for a flat orientation of ICD adsorbing on the surface, whereas an upper limit value would be for a vertical adsorbing orientation. A simple model calculation in which ICD is approximated as a rectangular box with dimensions of 25 Å × 15 Å × 5.2 Å indicates that one Au_{nm} particle (10.6 nm) can accommodate ~95 (for flat orientation) or ~270 (for vertical orientation along the long side) ICD molecules for a full monolayer coverage. For 1.2×10^{15} dye molecules (the starting quantity), 1.3×10^{13} (for flat orientation) or 4.4×10^{12} (for vertical orientation along the long side) Au_{nm} particles would be needed to form a full monolayer coverage. In Figure 6, the end point of the titration curve shows that 6.8×10^{12} Au_{nm} particles were required to observe the complete quenching. The experimental result is remarkable by the fact that the end point falls between the two calculated values (1.3×10^{13} and 4.4×10^{12}), suggesting the likelihood of a tilt orientation of dye molecules on the nanocrystal surface.

The quantitative aspect for the fluorescence quenching is further examined by measurements with Au_{nm} particles of a slightly larger size (11.5 nm). Theoretically, the surface of one Au_{nm} particle would accommodate ~110 ICDs (in flat orientation). For a solution of 1.2×10^{15} ICD molecules (0.67 μM), a theoretical 100% quenching would require 1.1×10^{13} Au_{nm} particles. Figure 7 shows a set of data obtained according to this experimental design. Indeed, the addition of 7.1×10^{12} Au_{nm} particles to the solution of 1.2×10^{15} ICD molecules was shown to be sufficient to exhibit ~100% quenching, corresponding to ~170 ICD quenchers per nanoparticle.

The above observation suggests that dye molecules are unlikely to adsorb horizontally on the nanocrystal surface (~110 dye/Au_{nm}). If the dye molecule is adsorbed vertically, ~320 dye molecules are required for a full monolayer coverage on a nanoparticle. The comparison between experimental data and theoretical estimates further demonstrates the likelihood of a tilt orientation for the adsorption of ICDs on the particle surface. As reflected by the calculation results from the experimental data, the observation of the slightly slower quenching rate in the lower-concentration case is suggestive of the possibility of a more horizontal orientation of the dye molecule on the surface, which is a subject of our in-depth investigation.

As shown in Figure 8A, the fluorescence quenching is further analyzed as a function of Au_{nm} concentration. This set of data was analyzed in two quantitative ways. First, the quenching efficiencies were compared between the calculated and experimental data (Table 1). The calculation assumes that the surface of one Au_{nm} nanocrystal can in average accommodate ~200 ICDs by considering an average of flat and vertical orientations. In Table 1, the general trend for the calculated and experimental quenching efficiency data is quite consistent. The calculated quenching efficiency is slightly smaller than the experimental ones. For example, the addition of 3.5×10^{12} Au_{nm} particles into the dye solution is expected to quench 58.3% of the dyes in the theoretical calculation. The change in fluorescence intensity showed a quenching efficiency of 78%. Second, the fluorescence quenching of ICD was found to be linearly dependent on Au_{nm} concentration before reaching the end point of titration (<3.0 nM). On the basis of the above experimental results, the adsorption of ICD on the surface of the nanoparticle (Au_{nm}) can be considered to involve electrostatic interaction between the negatively charged carboxylates of citrates on Au_{nm} and the positively charged nitrogen moieties of ICD in a steady state equilibrium (eq 1), which is a much faster process than the assembly process.

$$\mathrm{ICD} + \mathrm{Au_{nm}} \leftrightarrow \mathrm{ICD_{ads}/Au_{nm}} \tag{1}$$

C_1 and θ_1 are used to stand for the concentration of ICD in the solution and the surface fractional coverage of ICD on the negatively charged sites of Au_{nm}, respectively. $\theta_1 = \Gamma_1/\Gamma_0$, where Γ_1 represents the surface coverage (moles per cm^2) of ICD and Γ_0 the maximum monolayer surface coverage, which was estimated to be 4.43×10^{-11} mol/cm^2 for the flat orientation or 1.33×10^{-10} (vertical orientation along the long side) and 2.21×10^{-10} mol/cm^2 (vertical orientation along the short side) for the vertical orientation. C_0 represents the initial concentration of ICD ($C_1 = C_0 - C_{ads}$). The equilibrium for eq 1 can be described by a Langmuir type isotherm, that is,

$$K = \frac{\theta_1}{(1-\theta_1)C_1} \tag{2}$$

K represents the equilibrium constant. Since the particle−dye interaction is dominant for the fluorescence quenching phenomenon, the contribution of intermolecular interactions can be ignored. Considering the relationship between the change of ICDs in the solution and those adsorbed on the Au_{nm} surface (the total surface area of the nanoparticles used = (no. of Au_{nm}) × (surface area of one particle) = $(N_0 C_{NP} V)(SA_{NP})$), we have $N_0 V (C_0 - C_1) = N_0 \theta_1 \Gamma_0 (N_0 C_{NP} V)(SA_{NP})$, where N_0 is Avogadro's number, V is the total volume of the solution, and C_{NP} is the concentration of Au_{nm}. Thus, we have

$$\theta_1 = \frac{(C_0 - C_1)}{\Gamma_0 C_{NP} SA_{NP} N_0} \tag{3}$$

By solving this equation for C_1 with the consideration that K is a very large number, we derive

$$C_1 = -(N_0 \Gamma_0 SA_{NP}) C_{NP} + (C_0 - 1/K) \tag{4}$$

It shows that the concentration of the dye is a linear function of the concentration of the nanoparticles. By further considering the concentration dependence of fluorescence intensity being measured, $I = k' b C_1$, where $k' = 2.3 \Phi P_0 \epsilon$,[43] b is the cell path length, Φ is the quantum yield, P_0 is the power of the incident light, and ϵ is the molar absorptivity of dye, we have

$$I = (-k' b N_0 \Gamma_0 SA_{NP}) C_{NP} + k' b (C_0 - 1/K) \tag{5}$$

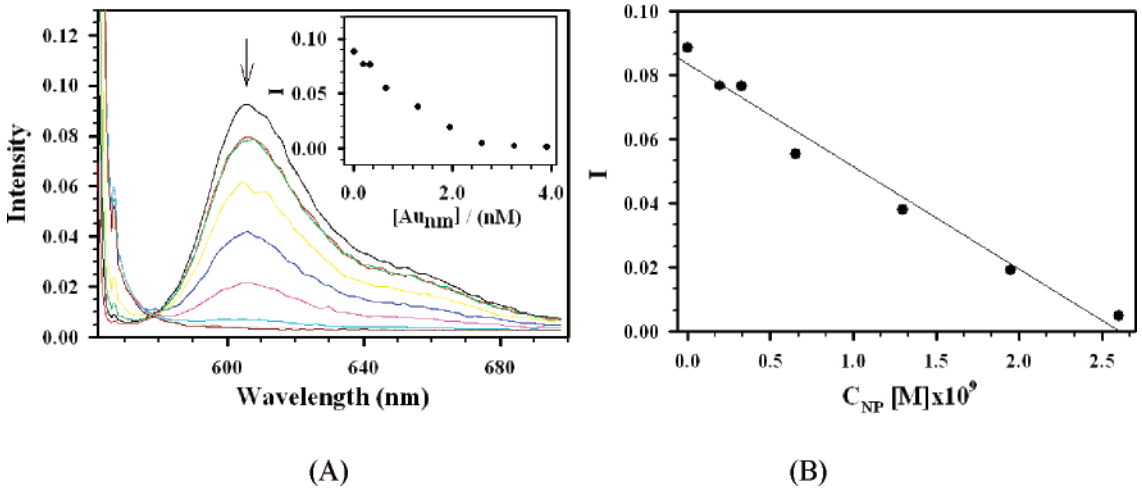

Figure 8. (A) Fluorescence spectra of ICD (0.67 μM) upon the addition of Au_{nm} (19.5 nM). Each spectrum was recorded 5 min after the addition of Au_{nm}. Inset: plot of the intensity (I) at 608 nm vs the concentration of Au_{nm}. The arrow indicates the direction of the spectral evolution with nanoparticle concentration. (B) Plot of the measured fluorescence intensity (I) at 608 nm vs the concentration of Au_{nm} (linear regression: $y = -3.20 \times 10^7 x + 0.083$).

TABLE 1: Analysis of the Fluorescence Quenching Data for a 0.67 μM Solution of Dye (1.2×10^{15} ICD) upon the Addition of Different Quantities of Au_{nm}

fluorescence intensity (608 nm[a])	no. of Au particles	% of dyes being quenched by Au (exptl[b])	% of dyes being quenched by Au (calcd[c])
0.089	0	0	0
0.077	3.5×10^{11}	13.4	5.8
0.077	5.9×10^{11}	13.7	9.6
0.055	1.2×10^{12}	37.5	19.5
0.038	2.4×10^{12}	56.9	38.3
0.019	3.5×10^{12}	78.3	58.3
0.005	4.7×10^{12}	94.5	78.2
0.002	5.9×10^{12}	97.6	97.6

[a] Baseline subtracted. [b] Based on the change in fluorescence intensity upon the addition of Au_{nm}. [c] The model calculation assumes that one Au_{nm} particle can adsorb 200 dye molecules for a full monolayer coverage.

Equation 5 shows a linear relationship between I and C_{NP} where the slope is $-k'bN_0\Gamma_0SA_{NP}$ and the y-intercept is $k'b(C_0 - 1/K)$. As shown by Figure 8B, this relationship fits quite well with the experimental data. Using the slope and intercept values obtained, and other parameters, $C_0 = 6.67 \times 10^{-7}$ M, $\Gamma_0 = 4.43 \times 10^{-11}$ mol/cm^2 (as described earlier), and $SA_{NP} = 4.17 \times 10^{-12}$ cm^2, we found $k'b$ to be 2.87×10^5 M^{-1} and K to be 2.65×10^6 M^{-1}. The latter shows indeed a large magnitude for the equilibrium constant, consistent with the fact that the adsorption of ICDs on the nanoparticle surface is thermodynamically favorable.

The quantum yield (Φ) is further estimated under the experimental conditions based on the experimental data. Using tetraphenylporphyrin (TPP) dissolved in benzene (3.45×10^{-5} M) as a standard (λ_{ex}, 550 nm; λ_{em}, 608 nm; Φ, 0.11; ϵ, 7.3×10^3 M^{-1} cm^{-1}), P_0 (=23.5) was obtained from the measured peak intensity ($I_{658nm} = 1.492$). The value of Φ, based on $k' = 2.3\Phi P_0\epsilon$, was estimated to be 0.05. If the linear regression data for $[Au_{nm}] < 1.6$ nM (slope -3.88×10^7) were used, the Φ value would be 0.06. In a separate measurement of TPP and ICD in the absence of nanoparticles under the same conditions, the peak intensity ($I_{610nm} = 2.935$) for a dye solution of 2.66×10^{-6} M yields a Φ value of 0.18, which is larger by a factor of $\sim$3 than that determined in the presence of nanoparticles, which reflects the significant effect of dye$-Au_{nm}$ interactions. This effect was further examined under a higher initial concentration of dye, as shown in Figure 6 ([ICD] = 1 μM). There was a slight volume increase due to the incremental addition of Au_{nm} solution into the solution of ICD, but it can be corrected on the basis of the linear dependence of intensity on concentration (see the Supporting Information); the value of Φ was found to be 0.25, which is larger by a factor of $\sim$1.5 than that obtained in the absence of nanoparticles ($\Phi = 0.16$). The results of these estimates, while varying within the experimental error range, demonstrated the important role played by the ICD$-Au_{nm}$ interactions in the solution. The dependence of fluorescence quenching on particle size was also examined (see the Supporting Information) and suggested that the fluorescence intensity decreases as the core size of Au_{nm} increases.

Conclusions

In conclusion, we have demonstrated a unique combination of nanoparticles and dyes for studying the interparticle interactions and reactivities. The combination of the indolenine cyanine dyes and the gold nanoparticles is shown to form a J-aggregate bridged assembly of nanoparticles, in addition to hydrophobic interparticle and electrostatic dye$-$particle interactions. Such interparticle interactions and reactivities are studied by probing the absorption of J-aggregates and fluorescence from the dyes and the surface plasmon resonance from the nanoparticles. The J-aggregation of the dyes adsorbed on the nanoparticles is shown to play an important role in the assembly of nanoparticles. The spectral evolution of the J-band of the dyes and the surface plasmon resonance band of the nanoparticles was found to be sensitive to the nature of the charge and the structure of the dyes. The fluorescence quenching for the dyes was shown to be quantitatively related to the surface coverage of the dyes on the nanocrystal surfaces. These findings have provided important information for assessing a two-step process involving a rapid adsorption of the dyes on the nanoparticles and a subsequent assembly of the nanoparticles involving a combination of interparticle J-aggregation and hydrophobic interactions of the adsorbed dyes. In view of the electrostatic nature for the adsorption of dyes and the weak molecular interactions for the interparticle J-aggregation, the optical or spectroscopic properties are expected to be tunable by molecules that regulate the electrostatic, hydrophobic, and $\pi-\pi$ interactions, or display specific recognition capabilities to the interaction sites. On the basis of our recent experience in using the dynamic light

scattering technique to probe nanoparticle assemblies in solution,[7a] part of our ongoing work is to address the issues related to the hydrodynamic sizes of the nanoparticle assemblies in the dye−nanoparticle system. Another part of our ongoing work also involves the delineation between the tunable optical or spectroscopic properties and the detailed nanostructures for developing spectroscopic nanoprobes for bioanalytical or biomedical applications and constructing devices with photochemical sensory properties.

Acknowledgment. This work is supported by the National Science Foundation (CHE 0349040) and in part the 3M Corporation. We also thank Mr. H. H. Eichelberger (Department of Biology, SUNY-Binghamton) for assistance in the TEM measurements. I-I. S. L. acknowledges the support of the National Science Foundation Graduate Research Fellowship.

Supporting Information Available: Discussions on NMR analysis, spectral evolution in the presence of tetrabutylammonium, salt concentration effect, FTIR analysis, and additional fluorescence data. This material is available free of charge via the Internet at http://pubs.acs.org.

References and Notes

(1) (a) Hostetler, M. J.; Green, S. J.; Stokes, J. J.; Murray, R. W. *J. Am. Chem. Soc*. **1996**, *118*, 4212. (b) Hostetler, M. J.; Templeton, A. C.; Murray, R. W. *Langmuir* **1999**, *15*, 3782. (c) Templeton, A. C.; Hostetler, M. J.; Kraft, C. T.; Murray, R. W. *J. Am. Chem. Soc*. **1998**, *120*, 1906. (d) Templeton, A. C.; Hostetler, M. J.; Warmoth, E. K.; Chen, S.; Hartshorn, C. M.; Krishnamurthy, V. M.; Forbes, M. D. E.; Murray, R. W. *J. Am. Chem. Soc*. **1998**, *120*, 4845.

(2) (a) Musick, M. D.; Pena, D. J.; Botsko, S. L.; McEvoy, T. M.; Richardson, J. N.; Natan, M. J. *Langmuir* **1999**, *15*, 844. (b) Zamborini, F. P.; Hicks, J. F.; Murray, R. W. *J. Am. Chem. Soc.* **2000**, *122*, 4514. (c) Templeton, A. C.; Zamborini, F. P.; Wuelfing, W. P.; Murray, R. W. *Langmuir* **2000**, *16*, 6682.

(3) (a) Mirkin, C. A.; Letsinger, R. L.; Mucic, R. C.; Storhoff, J. J. *Nature* **1996**, *382*, 607. (b) Elghanian, R.; Storhoff, J. J.; Mucic, R. C.; Letsinger, R. L.; Mirkin, C. A. *Science* **1997**, *277*, 1078. (c) Taton, T. A.; Mucic, R. C.; Mirkin, C. A.; Letsinger, R. L. *J. Am. Chem. Soc.* **2000**, *122*, 6305.

(4) (a) Boal, A. K.; Ilhan, F.; DeRouchey, J. E.; Thurn-Albrecht, T.; Russell, T. P.; Rotello, V. M. *Nature* **2000**, *404*, 746. (b) Boal, A. K.; Rotello, V. M. *J. Am. Chem. Soc.* **2002**, *124*, 5019. (c) Frankamp, B. L.; Boal, A. K.; Rotello, V. M. *J. Am. Chem. Soc.* **2002**, *124*, 15146. (d) Srivastava, S.; Frankamp, B. L.; Rotello, V. M. *Chem. Mater*. **2005**, *17*, 487.

(5) Kariuki, N. N.; Han, L.; Ly, N. K.; Patterson, M. J.; Maye, M. M.; Liu, G.; Zhong, C. J. *Langmuir* **2002**, *18*, 8255.

(6) (a) Leibowitz, F. L.; Zheng, W. X.; Maye, M. M.; Zhong, C. J. *Anal. Chem*. **1999**, *71*, 5076. (b) Zheng, W. X.; Maye, M. M.; Leibowitz, F. L.; Zhong, C. J. *Anal. Chem*. **2000**, *72*, 2190. (c) Han, L.; Luo, J.; Kariuki, N. N.; Maye, M. M.; Jones, V. W.; Zhong, C. J. *Chem. Mater*. **2003**, *15*, 29.

(7) (a) Maye, M. M.; Lim, I.-I. S.; Luo, J.; Rab, Z.; Rabinovich, D.; Liu, T.; Zhong, C. J. *J. Am. Chem. Soc.* **2005**, *127*, 1519. (b) Lim, I.-I. S.; Maye, M. M.; Luo, J.; Zhong, C. J. *J. Phys. Chem. B* **2005**, *109*, 2578.

(8) Han, L.; Daniel, D. R.; Maye, M. M.; Zhong, C. J. *Anal. Chem.* **2001**, *73*, 4441.

(9) (a) Zamborini, F. P.; Leopold, M. C.; Hicks, J. F.; Kulesza, P. J.; Malik, M. A.; Murray, R. W. *J. Am. Chem.* Soc. **2002**, *124*, 8958. (b) Leopold, M. C.; Donkers, R. L.; Georganopoulou, D.; Fisher, M.; Zamborini, F. P.; Murray, R. W. *Faraday Discuss.* **2004**, *125*, 63.

(10) Israel, L. B.; Kariuki, N. N.; Han, L.; Maye, M. M.; Luo, J.; Zhong, C. J. *J. Electroanal. Chem.* **2001**, *517*, 69.

(11) Narayanan, R.; El-Sayed, M. A. *J. Am. Chem. Soc*. **2004**, *126*, 7194.

(12) (a) Zhong, C. J.; Luo, J.; Maye, M. M.; Han, L.; Kariuki, N. N. Nanostructured Gold and Alloy Electrocatalysts. In *Nanotechnology in Catalysis*; Zhou, B., Hermans, S., Somorjai, G. A., Eds.; Kluwer Academic/Plenum Publishers: New York, 2004; Vol. 1, Chapter 11, pp 222−248. (b) Zhong, C. J.; Maye, M. M. *Adv. Mater.* **2001**, *13*, 1507.

(13) (a) Chen, S. *Langmuir* **2001**, *17*, 6664. (b) Chen, S. *J. Am. Chem. Soc.* **2000**, *122*, 7420. (c) Chen, S.; Yang, Y. *J. Am. Chem. Soc.* **2002**, *124*, 5280. (d) Hicks, J. F.; Zamborini, F. P.; Osisek, A. J.; Murray, R. W. *J. Am. Chem. Soc.* **2001**, *123*, 7048.

(14) Zheng, W. X.; Maye, M. M.; Leibowitz, F. L.; Zhong, C. J. *Analyst* **2000**, *125*, 17.

(15) Huang, T.; Murray, R. W. *Langmuir* **2002**, *18*, 7077.

(16) Ghosh, S. K.; Pal, A.; Kundu, S.; Nath, S.; Pal, T. *Chem. Phys. Lett.* **2004**, *395*, 366.

(17) (a) Li, H.; Rothberg, L. J. *J. Am. Chem. Soc*. **2004**, *126*, 10958. (b) Li, H.; Rothberg, L. J. *Anal. Chem*. **2004**, *76*, 5414.

(18) (a) Nicewarner-Pena, S. R.; Freeman, R. G.; Reiss, B. D.; He, L.; Pena, D. J.; Walton, I. D.; Cromer, R.; Keating, C. D.; Natan, M. J. *Science* **2001**, *294*, 137. (b) Nicewarner-Pena, S. R.; Carado, A. J.; Shale, K. E.; Keating, C. D. *J. Phys. Chem. B* **2003**, *107*, 7360.

(19) Maxwell, D. J.; Taylor, J. R.; Nie, S. *J. Am. Chem. Soc.* **2002**, *124*, 9606.

(20) Lian, W.; Litherland, S. A.; Badrane, H.; Tan, W.; Wu, D.; Baker, H. V.; Gulig, P. A.; Lim, D. V.; Jin, S. *Anal. Biochem.* **2004**, *334*, 135.

(21) (a) Thomas, K. G.; Kamat, P. V. *Acc. Chem. Res.* **2003**, *36*, 888. (b) Chandrasekharan, N.; Kamat, P. V.; Hu, J.; Jones, G., II. *J. Phys. Chem. B* **2000**, *104*, 11103. (c) Barazzouk, S.; Kamat, P. V.; Hotchandani, S. *J. Phys. Chem. B* **2005**, *109*, 716. (d) Nasr, C. P.; Liu, D.; Hotchandani, S.; Kamat, P. V. *J. Phys. Chem*. **1996**, *100*, 11054.

(22) (a) Gu, T.; Whitesell, J. K.; Fox, M. A. *Chem. Mater*. **2003**, *15*, 1358. (b) Hranisavljevic, J.; Dimitrijevic, N. M.; Wurtz, G. A.; Wiederrecht, G. P. *J. Am. Chem. Soc.* **2002**, *124*, 4536.

(23) (a) Wang, G. L.; Zhang, J.; Murray, R. W. *Anal. Chem.* **2002**, *74*, 4320. (b) Huang, T.; Murray, R. W. *J. Phys. Chem. B* **2001**, *105*, 12498. (c) Templeton, A. C.; Cliffel, D. E.; Murray, R. W. *J. Am. Chem. Soc.* **1999**, *121*, 7081.

(24) Dulkeith, E.; Ringler, M.; Klar, T. A.; Feldmann, J.; Munoz Javier, A.; Parak, W. J. *Nano Lett*. **2005**, *5*, 585.

(25) Randolph, J. B.; Waggoner, A. S. *Nucleic Acids Res.* **1997**, *25*, 2923.

(26) Sayama, K.; Hara, K.; Ohga, Y.; Shinpou, A.; Suga, S.; Arakawa, H. *New J. Chem.* **2001**, *25*, 200.

(27) Birch, M.; Bosworth, N.; Briggs, M.; George, J.; Scott, B. The Fourth International Symposium on Functional Dyes, Osaka, Japan, 1999.

(28) (a) Kobayashi, T., Ed. *J-Aggregates*; World Scientific Publishing Co.: Singapore, 1996. (b) Hannah, K. C.; Armitage, B. A. *Acc. Chem. Res*. **2004**, *37*, 845.

(29) (a) Lu, L. D.; Jones, R. M.; McBranch, D.; Whitten, D. *Langmuir* **2002**, *18*, 7706. (b) Jones, R. M.; Lu, L. D.; Helgeson, R.; Bergstedt, T. S.; McBranch, D. W.; Whitten, D. G. *Proc. Natl. Acad. Sci. U.S.A.* **2001**, *98*, 14769.

(30) Kerker, M. *J. Colloid Interface Sci*. **1985**, *105*, 297.

(31) Kometani, N.; Tsubonishi, M.; Fujita, T.; Asami, K.; Yonezawa, Y. *Langmuir* **2001**, *17*, 578.

(32) Wiederrecht, G. P.; Wurtz, G. A.; Hranisavljevic, J. *Nano Lett*. **2004**, *4*, 2121.

(33) Ghosh, S. K.; Pal, A.; Nath, S.; Kundu, S.; Panigrahi, S.; Pal, T. *Chem. Phys. Lett.* **2005**, *412*, 5.

(34) Makarova, O. V.; Ostafin, A. E.; Miyoshi, H.; Norris, J. R.; Miesel, D. *J. Phys. Chem. B* **1999**, *103*, 9080.

(35) Templeton, A. C.; Wuelfing, W. P.; Murray, R. W. *Acc. Chem. Res*. **2000**, *33*, 27.

(36) Verwey, E. J. W.; Overbeek, J. T. G. *Theory of the Stability of Lyophobic Colloids: The Interaction of Sol Particles Having an Electric Double Layer*; Elsevier: New York, 1948.

(37) (a) Li, Q.; Tan, J.; Peng, B. *Molecules* **1997**, *2*, 91. (b) Hamer, F. M. *The Cyanine Dyes and Related Compounds*; Wiley & Sons: New York, 1964; Vol. 18.

(38) Grabar, K. C.; Freeman, R. G.; Hommer, M. B.; Natan, M. J. *Anal. Chem*. **1995**, *67*, 735.

(39) Maye, M. M.; Han, L.; Kariuki, N. N.; Ly, N. K.; Chan, W.-B.; Luo, J.; Jones, V. W.; Zhong, C. J. *Anal. Chim. Acta* **2003**, *496*, 17.

(40) An, B.-K.; Kwon, S.-K.; Jung, S.-D.; Park, S. Y. *J. Am. Chem. Soc.* **2002**, *124*, 14410.

(41) Knapp, E. W. *Chem. Phys*. **1984**, *85*, 73.

(42) Zhang, F. X.; Han, L.; Israel, L. B.; Daras, J. G.; Maye, M. M.; Ly, N. K.; Zhong, C. J. *Analyst* **2002**, *127*, 462.

(43) (a) Lakowicz, J. R. *Principles of Fluorescence Spectroscopy*, 2nd ed.; Kluwer Academic/Plenum Press: New York, 1999. (b) Skoog, D. A.; Holler, F. J.; Nieman, T. A. *Principles of Instrumental Analysis*; Saunders College Pub.: Philadelphia, PA, 1998.